



This is a repository copy of *Being positive is not everything – experimental and computational studies on the selectivity of a self-assembled, multiple redox-state receptor that binds anions with up to picomolar affinities.*

White Rose Research Online URL for this paper:

<https://eprints.whiterose.ac.uk/185760/>

Version: Accepted Version

---

**Article:**

Zubi, A., Alnafisah, H.A., Turega, S. et al. (4 more authors) (2022) Being positive is not everything – experimental and computational studies on the selectivity of a self-assembled, multiple redox-state receptor that binds anions with up to picomolar affinities. *Chemistry – A European Journal*, 28 (5). e202102465. ISSN 0947-6539

<https://doi.org/10.1002/chem.202102465>

---

This is the peer reviewed version of the following article: A. Zubi, H. A. Alnafisah, S. Turega, I. Marques, J. R. B. Gomes, J. A. Thomas, V. Félix, *Chem. Eur. J.* 2022, 28, e202102465, which has been published in final form at <https://doi.org/10.1002/chem.202102465>. This article may be used for non-commercial purposes in accordance with Wiley Terms and Conditions for Use of Self-Archived Versions. This article may not be enhanced, enriched or otherwise transformed into a derivative work, without express permission from Wiley or by statutory rights under applicable legislation. Copyright notices must not be removed, obscured or modified. The article must be linked to Wiley's version of record on Wiley Online Library and any embedding, framing or otherwise making available the article or pages thereof by third parties from platforms, services and websites other than Wiley Online Library must be prohibited.

Items deposited in White Rose Research Online are protected by copyright, with all rights reserved unless indicated otherwise. They may be downloaded and/or printed for private study, or other acts as permitted by national copyright laws. The publisher or other rights holders may allow further reproduction and re-use of the full text version. This is indicated by the licence information on the White Rose Research Online record for the item.

**Takedown**

If you consider content in White Rose Research Online to be in breach of UK law, please notify us by emailing [eprints@whiterose.ac.uk](mailto:eprints@whiterose.ac.uk) including the URL of the record and the reason for the withdrawal request.



[eprints@whiterose.ac.uk](mailto:eprints@whiterose.ac.uk)  
<https://eprints.whiterose.ac.uk/>

# Being positive is not everything – experimental and computational studies on the selectivity of a self-assembled, multiple redox-state, receptor that binds anions with up to picomolar affinities

Ahmed Zubi,<sup>[a,b]</sup> Hawazin A Alnafisah,<sup>[a,c]</sup> Simon Turega,<sup>[d]</sup> Igor Marques,<sup>[e]</sup> José R. B. Gomes,<sup>[e]</sup> Jim A. Thomas,<sup>\*[a]</sup> and Vítor Félix<sup>\*[e]</sup>

[a] Dr Ahmed Zubi, Ms Hawazin A Alnafisah, Prof Jim A Thomas  
Department of Chemistry  
University of Sheffield  
Brook Hill, Sheffield, S3 7HF, UK  
E-mail: james.thomas@sheffield.ac.uk

[b] Chemistry Department, Faculty of Science,  
Misurata University, Misurata, Libya

[c] Department of Chemistry,  
Princess Nourah Bint Abdulrahman University, Riyadh, Saudi, Arabia

[d] Dr Simon Turega, Department of Bioscience and Chemistry,  
Sheffield Hallam University, Howard Street, Sheffield, S1 1WB, UK

[e] Dr Igor Marques, Dr José R. B. Gomes, Prof Vítor Félix, CICECO – Aveiro Institute of Materials, Department of Chemistry,  
University of Aveiro, 3810-193, Aveiro, Portugal  
E-mail: james.thomas@sheffield.ac.uk

Supporting information for this article is given via a link at the end of the document.

**Abstract:** The interaction of the self-assembled trinuclear ruthenium bowl  $1^{3+}$ , that displays three other accessible oxidation states, with oxo-anions is investigated. Using a combination of NMR and electrochemical experimental data, estimates of the binding affinities of  $1^{4+}$ ,  $1^{5+}$ , and  $1^{6+}$  for both halide and oxo-anions were derived. This analysis revealed that, across the range of oxidation states of the host, both high anion binding affinities ( $>10^9 M^{-1}$  for specific guests bound to  $1^{6+}$ ) and high selectivities (a range of  $>10^7 M^{-1}$ ) were observed. As the crystal structure of binding of the hexafluorophosphate anion revealed that the host has two potential binding sites (named the  $\alpha$  and  $\beta$  pockets), the host-guest properties of both putative binding sites of the bowl, in all of its four oxidation states, were investigated through detailed quantum-based computational studies. These studies revealed that, due to the interplay of ion-ion interactions, charge-assisted hydrogen-bonding and anion- $\pi$  interactions, binding to the  $\alpha$  pocket is generally preferred, except for the case of the relatively large and lipophilic hexafluorophosphate anionic guest and the host in the highest oxidation states, where the  $\beta$  pocket becomes relatively favourable. This analysis confirms that host-guest interactions involving structurally complex supramolecular architectures are driven by a combination of non-covalent interactions and, even in the case of charged binding pairs, simple ion-ion interactions alone cannot accurately define these recognition processes.

## Introduction

As anions have important roles in a spectrum of areas within biology and the environment, their detection is an increasingly important research subject.<sup>[1–5]</sup> As a consequence, the coordination chemistry of anions and their binding by specifically designed receptors and sensors has burgeoned over the last two

decades.<sup>[6–13]</sup> However, the difficulties inherent in the non-covalent recognition of anions are well known: when compared to analogous cations they are larger and have lower charge densities; they possess a wider spectrum of shapes; anions may only exist within a specific pH range; and tend to have higher free energies of solvation.<sup>[14][15]</sup>

For these reasons, macrocyclic structures are frequently targeted in the construction of anion receptors as these architectures often display greater selectivities and higher affinities than other host designs.<sup>[16–22]</sup> Furthermore, if these hosts are optically or electrochemically active, so that they can supply an output for the recognition process, they can also function as sensors for their anionic guests.<sup>[23–26]</sup> The difficulty in this approach lies in the challenging multistep syntheses required to isolate such structurally complex 3D hosts.<sup>[26–27]</sup> An alternative approach that has been much pursued involves self-assembly, with metal ion-directed approaches being particularly fruitful.<sup>[27–34]</sup>

Another area of coordination chemistry research that has a longer history is focused on mixed-valence (MV) transition metal complexes. Through experimental and theoretical work, MV systems have been intensely studied for approximately fifty years as they provide insights into the nature of electron transfer processes.<sup>[35–41]</sup> This has led to a deeper understanding of many complex, redox-based, biological processes, including photosynthesis. MV systems have also formed the basis of several forms of molecular devices.<sup>[42–47]</sup> The prototype synthetic MV system is the Creutz-Taube ion (CT ion).<sup>[35]</sup> This apparently simple species illustrates the complexities of MV systems. Using a classification delineated by Robin and Day,<sup>[48]</sup> it was first thought that the CT ion was either a Class II (valence localised, electron hoping) or Class III (valence delocalised) system. However, after several decades of research, involving many groups and a wide range of experimental and computational techniques, Meyer and

colleagues suggested that the CT ion is a hybrid, valence localised/solvation sphere averaged Class II/III system.<sup>[38]</sup>

As part of a program to develop novel systems for the recognition of anions,<sup>[49]</sup> bio-anions,<sup>[50]</sup> and biomolecules,<sup>[51–55]</sup> the Thomas group has been investigating the self-assembly of oligonuclear metallomacrocycles, such as the trinuclear macrocyclic bowl  $1^{3+}$  (Fig. 1), assembled from  $Ru^{II}([9]aneS_3)$  fragments and 9-methyladenine (9MA) bridging ligands.<sup>[56–58]</sup> An understanding of the host-guest properties of this redox-active system requires insights from both of the research areas described above.

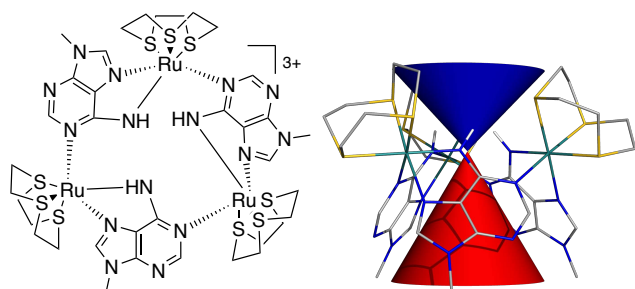


**Fig. 1.** Structure of macrocycle  $1^{3+}$  (left) with the  $\alpha$  and  $\beta$  pockets (right) depicted as blue and red cones, respectively. The C–H hydrogen atoms were hidden for clarity.

Although the macrocycle is isolated as a  $Ru^{III}_3$  complex, it is oxidised to its  $Ru^{II}_3$  state in three electrochemical steps, going through two separate –  $[Ru^{II}_2Ru^{III}]$  and  $[Ru^{II}Ru^{II}]$  – MV states. Surprisingly, due to the novel connectivity of metal centers and bridging ligands within the MV structures, it is a Class II system in the  $[Ru^{II}_2Ru^{III}]$  state, but a Class III system in the  $[Ru^{II}Ru^{II}]$  state.<sup>[56]</sup> The host-guest properties of the macrocycle and their effect on its redox properties have been investigated. These studies revealed a unique phenomenon: without any concomitant change in potential, anions can be used to switch the assembly from one mixed valence state to another, a process that is driven by the host-guest chemistry of the macrocycle.<sup>[56]</sup> These initial studies were carried out using halide anions – chosen because their simple spherical geometry allowed to investigate the effect of size on guest binding and were compared to the host's interaction with the nonpolar tetrahedral  $ClO_4^-$  anion, which was found to be very weak.

NMR studies revealed that  $1^{3+}$  binds halide ions in a 1:1 stoichiometry and displays good selectivity for intermediate sized guests:  $>10^5 M^{-1}$  for chloride, but  $<300 M^{-1}$  for fluoride. Although the metallomacrocyclic has two possible binding pockets – an  $\alpha$  pocket defined by the thiacrown ligands and the N–H binding sites from 9MA units (illustrated in Fig. 1 by the blue cone), and a  $\beta$  pocket defined by 9MA bridging ligands (illustrated in Fig. 1 by the red cone) projecting out to give a bowl shaped aromatic surface – both the NMR studies and the crystal structure of  $[1]Br_3$  indicated that the macrocycle binds halide guests exclusively in the  $\alpha$ -binding pocket. Recognition of these anions entails a panoply of hydrogen bonds largely involving ethylenic C–H residues of the coordinated thiacrown ligands that define the lip of the pocket. However, the N–H moieties of the three 9MA bridging ligands form a tridentate “N–H pincer” suited to bind larger anions and form complementary hydrogen-bond to suitable accepting moieties. Hence, we sought to extend these studies and investigate the host-guest chemistry of  $1^{3+}$  with larger, structurally

more complex, oxo-anions. With these experimental data to hand, we constructed a detailed, quantum-based analysis of the host's interaction with anions, which allowed us to dissect the forces that drive the recognition processes in the different redox states of the host.

## Results and Discussion

### NMR studies

Previous studies have shown that the host binds nonpolar, more structurally complex, anions like perchlorate and hexafluorophosphate ions weakly in solution.<sup>[56–58]</sup> Here, we extend our studies to investigate more polar, potentially hydrogen bonding, oxo-anion guests. So that the effect of geometry, charge, and size could be explored, a mixture of tetrahedral ions and trigonal oxo-anions were chosen. We initially intended to extend these studies to dianions, however this was not possible as the host rapidly precipitated on the addition of guests such as  $SO_4^{2-}$ .  $^1H$ -NMR titrations with the selected anions in  $d_3$ -MeCN all revealed distinctive changes in the spectra of the host – Table 1. In particular, the N–H protons of the 9MA bridging ligand showed downfield shifts that are characteristic of binding into the same cavity as halide ion guests. Furthermore, the intensity of these shifts was highly dependent on the nature of the guest. The largest shift, of 0.95 ppm, was observed for  $CH_3COO^-$ , whilst the smallest (0.22 ppm) – induced by  $HSO_4^-$  – was almost comparable to that observed for perchlorate (0.12 ppm). In fact, the range of these values are less than those obtained for halide guests, which stretch from 3.65 ppm ( $F^-$ ) to 0.52 ppm ( $I^-$ ); however, a closer analysis of these data reveals that the two  $sp^2$ -based trigonal anions all produced larger shifts than the  $sp^3$ -based tetrahedral anions – Table 1.

**Table 1.** – Anion guest induced  $^1H$ -NMR shifts in the N–H signals on 9MA bridging ligands of host  $1^{3+}$  and the  $K_a$  estimates for 1:1 anion binding derived from these data.<sup>[a]</sup>

Anion	$\Delta \delta$ /ppm	$K_a/M^{-1}$
$CH_3COO^-$	0.95	720
$HSO_4^-$	0.22	1200
$NO_3^-$	0.52	260
$H_2PO_4^-$	0.27	490
$ClO_4^-$	0.12	120

[a] To aid comparisons, data for  $ClO_4^-$  previously reported in ref. <sup>[58]</sup> is also included.

As for the halide guests, oxo-anions cause tell-tale shifts in both the bridging ligands and the thiacrown-based signals, which further confirm they bind in the same site as halide ions (see Figs. S1–S5). Using the shifts in the N–H protons of the 9MA bridging ligands, binding curves for the interaction with each guest were constructed, as illustrated in Fig. S6 with the binding curve fit and associated Job plot for acetate. Estimated association binding constant ( $K_a$ ) values are summarised in Table 1.

As for our previous studies,<sup>[58]</sup> there is not a direct correlation between the magnitude of signal shifts – which actually reflect polarization – and the binding affinities. For the structurally

complex anions studied herein, the binding affinity for hydrogen sulfate is the highest. Despite having a lower charge density than halide anions, the overall affinity for this anion is comparable to those reported for some of the halides and, while affinities for the other oxo species are lower, they are similar in magnitude to the value reported for the interaction with fluoride guest, the halide with the lowest binding affinity ( $283 \text{ M}^{-1}$ ). The trend in affinities does not simply map onto the size of the guest, but loosely correlates with the Lewis base strengths of the anions, indicating that hydrogen bond interactions are involved in the recognition process. Taken with the pattern of observed NMR shifts, these data are consistent with binding to the same receptor site involved in halide guest recognition.

### Binding affinities of higher oxidation states from electrochemical studies

Due to anion-induced precipitation at the concentrations required for cyclic voltammetry studies, titrations with only three of the oxo-anion guests – namely the acetate, nitrate, and perchlorate ions – were possible. However, these three guests do span a good range of oxo-anion binding affinities for the isoivalent  $\text{Ru}^{\text{II}}$  macrocycle, thus providing insights into the effect of the anions on the host's electrochemical response.

Unlike previous electrochemical studies involving halide ions that were complicated by the redox activity of the guests, on addition of oxo-anions, shifts in the three redox couples of host  $1^{n+}$  are straightforwardly detected using square wave voltammetry (see Figs. S7-S9). Each oxidation process of the host displays shifts that are characteristic of the individual guest employed, see Table S1 for a summary of these data.

In a previous study we pointed out that the  $1^{3+} - 1^{6+}$  redox chain is somewhat similar to a dynamic combinatorial library of host architectures in which host-guest interactions select for, and stabilize, the "best" host redox state.<sup>[58]</sup>

To investigate this issue in more detail, binding affinities for guests were estimated using methods first developed for redox active crown and cryptand hosts.<sup>[59–63]</sup> In this model, the electrochemical potentials of a free and bound host ( $E_{\text{H}}$  and  $E_{\text{HG}}$  respectively) and the binding affinity of its oxidation states ( $K_{\text{ared}}$  and  $K_{\text{aox}}$  respectively) are related in this way:

$$\frac{K_{\text{a}}(\text{red})}{K_{\text{a}}(\text{ox})} = e^{\left(\frac{F}{RT}\right)(E_{1/2}(\text{HG}) - E_{1/2}(\text{H}))}$$

Therefore, given the binding affinities of  $1^{3+}$  and the electrochemical shifts for generation of  $1^{4+}$  in the absence and presence of specific guests,  $K_{\text{a}}(1^{4+})$  values can be estimated through this relationship.

Once values for  $K_{\text{a}}(1^{4+})$  are obtained, these figures along with the second oxidation potential in the presence and absence of the specific guest, can provide an estimate of  $K_{\text{a}}(1^{5+})$ . Finally, this latter figure can be used with data for the third oxidation processes to estimate  $K_{\text{a}}(1^{6+})$ . The analyses of the data collected in this study and in our previous study involving halide ions are summarized in Table 2.

The results reveal that across the four oxidations states anion binding affinities span seven orders of magnitude, with selectivity towards halides being particularly apparent. A graphical comparison of these data reveals some interesting effects – Fig. 2. For example, affinities for the smallest anion, fluoride, show the simplest trend;  $K_{\text{a}}$  for  $\text{F}^-$  increases by two orders of magnitude for each increase in positive charge on the host, suggesting that the

increase in ion-ion interactions makes the largest contribution to enhanced binding. However, more complex trends are observed with other guests.

**Table 2.** – Estimated binding affinities for anions with metallo-macrocyclic host in different oxidation states.<sup>[a][b]</sup>

Guest	$K_{\text{a}}(1^{3+})$	$K_{\text{a}}(1^{4+})$	$K_{\text{a}}(1^{5+})$	$K_{\text{a}}(1^{6+})$
$\text{ClO}_4^-$	120	177	261	$1.02 \times 10^3$
$\text{NO}_3^-$	260	$1.8 \times 10^3$	$2.8 \times 10^4$	$1.6 \times 10^5$
$\text{CH}_3\text{COO}^-$	720	$1.3 \times 10^3$	$1.1 \times 10^5$	$1.1 \times 10^5$
$\text{F}^-$	285	$1.4 \times 10^4$	$1.5 \times 10^6$	$1.1 \times 10^8$
$\text{Cl}^-$	$1.6 \times 10^5$	$1.7 \times 10^7$	$1.5 \times 10^9$	$3.3 \times 10^9$
$\text{Br}^-$	$3.9 \times 10^4$	$4.9 \times 10^5$	$2.4 \times 10^6$	$1.6 \times 10^6$

[a] Binding affinities for the three halide anions were calculated using the electrochemical data obtained in ref 58. [b] Electrolyte: TBAPF6

Although  $1^{6+}$  binds chloride with picomolar affinity – figures that are comparable with some of the highest values for anion-binding receptors<sup>[22,64–66]</sup> – the interaction is still slightly lower than expected by the simple linear trend observed for  $1^{3+} - 1^{5+}$  with fluoride. More strikingly, although acetate is bound with the third highest affinity by all the redox states of the host, estimates of  $K_{\text{a}}(\text{CH}_3\text{COO}^-)$  for  $1^{6+}$  are identical to  $1^{5+}$ , confirming that the interaction of this host with larger and more complex anions is not simply driven by ion-ion and other electrostatic interactions. Indeed, there is an increased charge contribution to binding in  $1^{6+}$  compared to  $1^{5+}$  and yet they bind acetate with the same affinity. These observations insinuate that more specific host-guest interactions with this guest are optimized in the  $1^{5+}$  redox state.

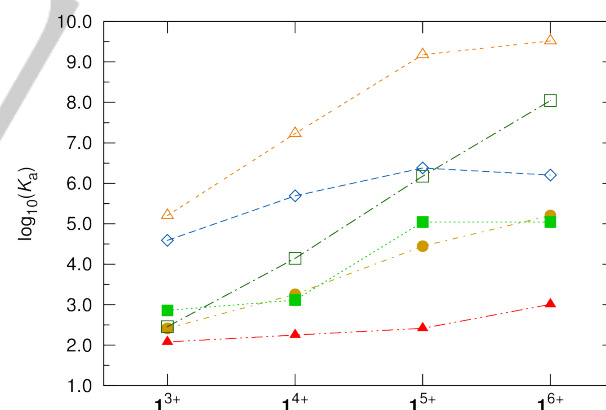


**Fig. 2.** Trends in estimated  $K_{\text{a}}$  values for the four different oxidation states of self-assembled host  $1^{n+}$  with  $\text{CH}_3\text{COO}^-$  (■),  $\text{NO}_3^-$  (●),  $\text{ClO}_4^-$  (▲),  $\text{F}^-$  (□),  $\text{Cl}^-$  (△), and  $\text{Br}^-$  (◇)

### Crystallographic Studies

To investigate the solid-state host properties of  $1^{3+}$  with structurally more complex anions, attempts were made to grow crystals of the host in the presence of all the oxo-anions and related counterions, but these were not successful. However, X-ray quality crystals of its hexafluorophosphate salt were obtained, which led to somewhat unexpected results.

## FULL PAPER

Surprisingly, the structure reveals that two anions make close contact with the macrocyclic cation – Fig. 3. Consistent with previous NMR studies, one anion is bound into the thiacycrown-based  $\alpha$ -face of the host, where an array of close contacts are made by hydrogen bond donor sites on the thiacycrown and the N–H groups of the 9MA bridging ligands to fluorine atoms on the anion. However, a second anion sits at the open  $\beta$ -face of the bowl making close contacts with hydrogens on the 9-methyl groups of the 9MA bridging ligands, confirming that – in the solid phase at least – this face can also be a host site for larger and/or more lipophilic anions. This observation also insinuates that anion- $\pi$  interactions<sup>[67–71]</sup> may play a part in the host-guest interactions of the macrocycle.

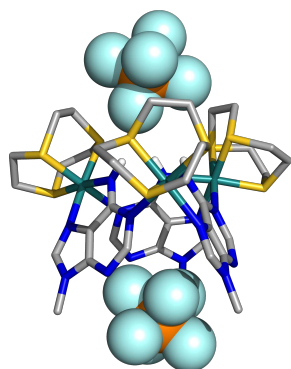


**Fig. 3.** Host-guest association observed in the crystal structure of  $[1](PF_6)_3$ , with two hexafluorophosphate anions lodged in the  $\alpha$  and  $\beta$  pockets of the metallomacrocyclic cation.

Unlike the previously reported structure with bromide anions, in which face-to-face macrocycles define a dimeric capsule, the interactions between the individual host cations and the two  $PF_6^-$  anions define hexagonal channels – Fig. S10A, which are occupied by the remaining  $PF_6^-$  anions – Fig. S10B.

The NMR binding data in MeCN and the crystallographic structure imply that anion binding by the macrocycle in its different oxidation states is not simply driven by a stepwise increase in ion-ion interactions between host and guest. This is consistent with previous studies indicating that anionic guest recognition by macrocyclic hosts is not primarily driven by straightforward ion-ion interactions in higher dielectric solvents like MeCN, but increasingly involves induction and dispersion forces. In our previous report we described initial computational studies that provided considerable insights into the interaction of  $1^{3+}$  with simple spherical halide anions. To investigate the issues described above in more detail, the interaction of each oxidation state of the macrocycle with oxo-anions were studied using computational approaches (*vide infra*). This work was further motivated by the fact that computational studies on the energetics of anion binding by metallomacrocycles are still rare. Indeed, as far as we are aware, this is the first comprehensive theoretical investigation on the anion binding properties of a self-assembled metallomacrocyclic host that exhibits multiple redox states for anion guests.

### Computational studies

To comprehensively analyze the host properties of  $1^{n+}$ , in its different oxidation states, Gaussian09<sup>[72]</sup> was used to perform extensive DFT calculations with a polarised continuous solvent

model (PCM)<sup>[73]</sup> of MeCN, using the CAM-B3LYP functional with Grimme's D3 dispersion correction,<sup>[74]</sup> coupled with the LANL2TZ(f) basis set for ruthenium and with the 6-31+G(d) basis set for the remaining elements.<sup>[75]</sup> Moreover, for the higher oxidation states, two alternative spin multiplicities were considered, 1 and 3 for  $1^{5+}$  and 2 and 4 for  $1^{6+}$ . Henceforth, these low- and high-spin species will be designated by  $ls-1^{5+}$  and  $ls-1^{6+}$ , and  $hs-1^{5+}$  and  $hs-1^{6+}$ , respectively. Further computational details, as well as additional Tables and Figures, are given in the ESI.

**Structure and spin states.** In the optimized structure of free  $1^{3+}$  (see Fig. S11), the computed Ru-S distances are equivalent and are indistinguishable between the three thiacycrown ethers, with an average value of  $2.360 \pm 0.006$  Å (Table S2). The Ru-N distances have identical values, independently of the bonded N atom and coordination mode of the 9MA bridging ligands, with an average value of  $2.152 \pm 0.007$  Å. In addition, while the Ru-N distances are identical to those observed in the single crystal X-ray structure of  $[1](PF_6)_3$ , the computed Ru-S distances are ca. 0.07 Å slightly longer. Along the subsequent oxidation states, the Ru-S distances successively increase 0.015 ( $1^{4+}$ ), 0.013 ( $1^{5+}$ ) and 0.011 Å ( $1^{6+}$ ), with an average value of  $2.398 \pm 0.019$  Å for the later oxidation state. On the other hand, the Ru-N average distances also change slightly, decreasing from  $1^{3+}$  ( $2.152 \pm 0.007$  Å) to  $1^{6+}$  ( $2.104 \pm 0.061$  Å). The Ru-S and Ru-N distances are independent of the spin multiplicities in the  $1^{5+}$  and  $1^{6+}$  hosts (Table S2).

The analysis of the Mulliken spin densities (Table 3) for the  $1^{n+}$  MV states confirms that the  $[Ru^{II}_2Ru^{III}]$  state ( $1^{4+}$ ) contains a single unpaired electron. For the subsequent  $[Ru^{II}Ru^{III}_2]$  MV state ( $1^{5+}$ ), in the diamagnetic low-spin configuration the spin densities show that the unpaired electrons of the two  $Ru^{III}$  centres have opposite spins, consistent with their coupling through the 9MA bridges, while in the high-spin state, naturally, no coupling is observed. In the  $1^{6+}$   $[Ru^{III}_3]$  host the spin densities indicate that the odd electrons in two  $Ru^{III}$  centres have opposite spins in  $ls-1^{6+}$ , while in  $hs-1^{6+}$  the three electrons of the  $Ru^{III}$  centers have the same spin. However, the difference between the electronic energies, corrected with the zero-point vibrational energies of  $ls-1^{6+}$  and  $hs-1^{6+}$  is only  $0.8$  kcal mol<sup>-1</sup>, while  $ls-1^{5+}$  and  $hs-1^{5+}$  are almost degenerate (see Table S3), indicating that both spin multiplicities for these oxidation states are likely.

**Table 3.** Mulliken spin densities on Ru centres in free  $1^{n+}$  ( $n = 4, 5$  or  $6$ ), with the corresponding electron configurations

Oxidation state	Mulliken spin densities (a.u.)	Electron configuration
$1^{4+}$	+0.001 ; +0.001 ; +0.685	$\uparrow\downarrow$ ; $\uparrow\downarrow$ ; $\uparrow$
$ls-1^{5+}$	-0.001 ; +0.784 ; -0.649	$\uparrow\downarrow$ ; $\uparrow$ ; $\downarrow$
$hs-1^{5+}$	+0.011 ; +0.777 ; +0.628	$\uparrow\downarrow$ ; $\uparrow$ ; $\uparrow$
$ls-1^{6+}$	+0.788 ; +0.755 ; -0.773	$\uparrow$ ; $\uparrow$ ; $\downarrow$
$hs-1^{6+}$	+0.781 ; +0.771 ; +0.774	$\uparrow$ ; $\uparrow$ ; $\uparrow$

**General anion binding analysis.** The anion binding properties for the four oxidation states of  $1^{n+}$  were initially ascertained from the electrostatic potential distribution mapped onto the electron density surface ( $V_s$ ) calculated with Multiwfn.<sup>[76,77]</sup> Overall, the most positive region of  $V_s$  covers the  $\alpha$  pocket including the [9]aneS<sub>3</sub> ligands, while the less positive region naturally encloses

the aromatic moieties of the 9MA bridging ligands of the  $\beta$  pocket, as illustrated in Fig. S12. The highest value of  $V_S$  ( $V_{S,max}$ , see Table S4) is found inside the  $\alpha$  pocket, near the “pincer” composed by the N–H binding units of the three 9MA bridges, and grows linearly with the oxidation state ( $R^2 = 1.000$ , Fig. S13). For each host oxidation state, the  $\beta$  pocket also displays a well-defined electrostatic potential region enclosing deeply buried high  $V_S$  points (Table S4), inaccessible to the anionic guests. On the other hand, the difference between the highly correlated  $\alpha$  and  $\beta$  highest  $V_S$  values ( $R^2 = 0.999$ , Fig. S13) decreases as oxidation state increases (Table S4), suggesting the possibility of anion recognition in the  $\beta$  pocket at least at the higher oxidation states of the host (*vide infra*).

Afterwards, the DFT calculations were continued with the oxo-anion associations of  $1^{n+}$ . In agreement with the experimental binding and structural data and the theoretical insights deduced from the  $V_S$  calculations,  $\text{CH}_3\text{COO}^-$ ,  $\text{NO}_3^-$ ,  $\text{ClO}_4^-$ ,  $\text{HSO}_4^-$  and  $\text{H}_2\text{PO}_4^-$  were positioned in the room provided by the  $\alpha$  pocket or, alternatively, by the  $\beta$  pocket, with the host in the four different oxidation states and spin multiplicities. Moreover, for acetate hosted in the  $\beta$  pocket, the anion was positioned with either the carboxylate or methyl groups pointing inwards the cavity, thus a total of 66 putative binding arrangements were generated and investigated. The optimised structures of  $1^{n+}$  with oxo-anions encapsulated in these two alternative binding scenarios are shown in Figs. S14–S24. Overall, the energy differences observed between the low- and high-spin states of  $1^{5+}$  and  $1^{6+}$  free hosts are maintained in their anion associations (see Table S3), with the low-spin  $1^{5+}$  and  $1^{6+}$  associations being slightly favoured. In agreement, unless otherwise stated, in the subsequent structural and energetic analyses, the  $1^{5+}$  and  $1^{6+}$  associations are discussed regardless of their alternative electronic configurations. Furthermore, the Mulliken spin densities observed in the free hosts are not perturbed by the anion binding (see Table S5). The binding enthalpy, at 298.15 K, for the host-guest associations ( $\Delta H_{HG}$ ) between  $1^{n+}$  and the anions was directly estimated from the structures of the host-guest, host, and guest DFT optimized in acetonitrile continuous solvent using Equation S1, as detailed in ESI. The  $\Delta H_{HG}$  values gathered in Table S6, indicate that the interactions between the  $1^{n+}$  hosts and the guest anions are stronger in the  $\alpha$  pocket than in the  $\beta$  site, *i.e.*, the oxo-anions are preferentially hosted in the former, in line with the  $^1\text{H-NMR}$  anion binding data (*vide supra*) for  $1^{3+}$  with the enthalpy differences between the  $\alpha$  and  $\beta$  oxo-anions hosted systems ranging from  $-20.4$  (*Is-1^{6+}*· $\text{CH}_3\text{COO}^-$ ) to  $-4.7$  kcal mol $^{-1}$  (*Is-1^{6+}*· $\text{ClO}_4^-$ ). Moreover, the values of binding enthalpy for each oxo-anion, regardless of the binding pocket, linearly increase with the host's oxidation state as illustrated in Fig. 4 for the associations with the anions hosted in the  $\alpha$  pocket of  $1^{n+}$ . Given the clear binding preference of the oxo-anions for the  $\alpha$  pocket, further analyses of the oxo-anions hosted at the  $\beta$  pocket were not performed.

The  $\Delta H_{HG}$  values computed for the oxo-anions hosted at the  $\alpha$  binding pocket show that the binding affinity order is not preserved along the host's oxidation states, changing from  $1^{3+}$  ( $\text{H}_2\text{PO}_4^- > \text{HSO}_4^- > \text{CH}_3\text{COO}^- \approx \text{ClO}_4^- > \text{NO}_3^-$ ), to  $1^{4+}$  ( $\text{H}_2\text{PO}_4^- > \text{CH}_3\text{COO}^- \approx \text{HSO}_4^- > \text{ClO}_4^- \approx \text{NO}_3^-$ ), to  $1^{5+}$  ( $\text{H}_2\text{PO}_4^- > \text{CH}_3\text{COO}^- \approx \text{HSO}_4^- > \text{NO}_3^- \approx \text{ClO}_4^-$ ), and finally to  $1^{6+}$  ( $\text{H}_2\text{PO}_4^- > \text{CH}_3\text{COO}^- > \text{HSO}_4^- > \text{NO}_3^- > \text{ClO}_4^-$ ). Overall, these binding enthalpy trends are not straightforwardly related with the nucleophilic character of the oxo-anions ascertained by the most negative values ( $V_{S,min}$ ) of

their electrostatic distributions, which follow the order (kcal mol $^{-1}$ ):  $\text{CH}_3\text{COO}^- (-176.0) > \text{H}_2\text{PO}_4^- (-148.1) > \text{NO}_3^- (-140.8) > \text{HSO}_4^- (-135.9) > \text{ClO}_4^- (-123.5)$ . However, when binding enthalpies of the tetrahedral and trigonal anions are separately analysed, the  $\Delta H_{HG}$  values mirror the  $V_{S,min}$  ones, following the same trend, independently of the host's oxidation state.

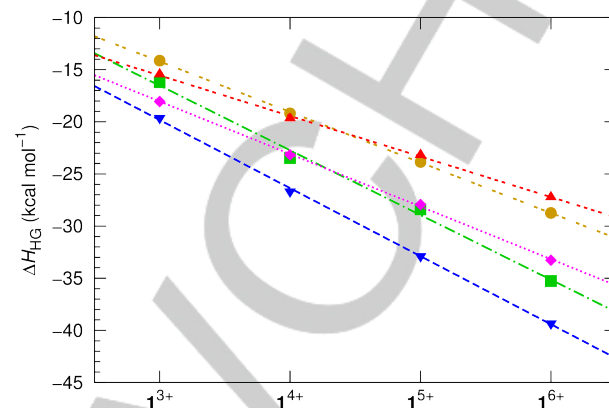


**Fig. 4.** Variation of the computed  $\Delta H_{HG}$  (kcal mol $^{-1}$ ) between  $1^{n+}$  and the oxo-anions in the  $\alpha$  pocket, together with the corresponding linear fits ( $R^2 \geq 0.995$ ). Key:  $\text{CH}_3\text{COO}^-$  (■),  $\text{NO}_3^-$  (●),  $\text{ClO}_4^-$  (▲),  $\text{HSO}_4^-$  (◆) or  $\text{H}_2\text{PO}_4^-$  (▼). The points for the high-spin electron configurations are not plotted as they would overlap with the low-spin configurations data.

Comparable predicted affinity trends are obtained with the binding free energies ( $\Delta G_{HG}^{SS}$ ), estimated using the thermochemistry analysis data summarised in Table S6 and corrected for reference state in solution (1 M). The contribution of the enthalpy for the binding free energy of all host-guest systems is larger than the  $T\Delta S$  term, indicating that the binding of the oxo-anions in the  $\alpha$  pocket is driven by the former energetic term.

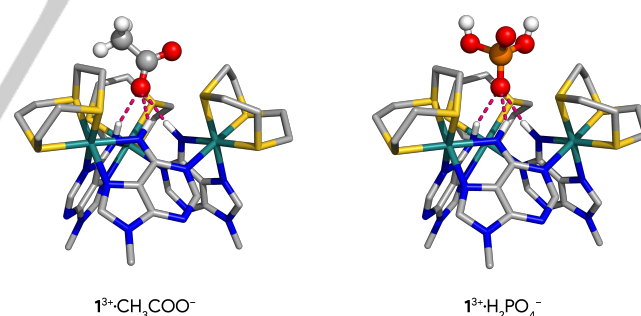


**Fig. 5** – DFT optimised structures of  $1^{3+}$  associations with  $\text{CH}_3\text{COO}^-$  and  $\text{H}_2\text{PO}_4^-$  hosted in pocket  $\alpha$ . The N–H...O hydrogen bonds are drawn as pink dashed lines. The hosts' C–H hydrogen atoms were hidden for clarity.

**Oxo anion binding analysis.** The volumes of the anionic guest were estimated from the electrostatic potential calculations (see ESI). The volume values ( $\text{\AA}^3$ ) for the oxo-anions and halide series follow the orders:  $\text{H}_2\text{PO}_4^- (96.97) > \text{HSO}_4^- (90.70) > \text{ClO}_4^- (85.90) > \text{CH}_3\text{COO}^- (85.20) > \text{NO}_3^- (66.23); \text{I}^- (72.41) > \text{Br}^- (58.33) > \text{Cl}^- (49.43) > \text{F}^- (28.28)$ . The volume of  $\text{PF}_6^-$  was calculated as  $97.72 \text{ \AA}^3$ . Regardless of the volume and binding geometry of the oxo-anions, a single oxygen atom is entirely embedded into the  $\alpha$  pocket and bonded through three convergent hydrogen bonds from the three N–H binding sites of  $1^{n+}$ , as illustrated in Fig. 5 for the  $1^{3+}$  host-guest systems with  $\text{CH}_3\text{COO}^-$  and  $\text{H}_2\text{PO}_4^-$ . The

## FULL PAPER

computed structures also display multiple C–H···O close contacts between the non-coordinated oxygen atoms and C–H groups from the thiacycrown ethers.

The average dimensions computed for the three N–H···O hydrogen bonds are summarised in Table S7, while the distance from the anion's central atom ( $A_c = S, P, N, Cl$  or  $C_{COO^-}$  in  $HSO_4^-$ ,  $H_2PO_4^-$ ,  $NO_3^-$ ,  $ClO_4^-$  or  $CH_3COO^-$ , respectively) to the  $N_3$  plane, determined by the three N atoms from the N–H groups of the 9MA bridging ligands, are reported in Table S8. The  $A_c \cdots N_3$  distances decrease with each increment of the host's positive charge, with the anions being progressively buried deeper in the  $\alpha$  pocket as a result of the charge-assisted hydrogen bonding interactions (*vide infra*). For instance, for the basic acetate, the  $A_c \cdots N_3$  distances go from 3.616 ( $1^{3+}$ ) to 3.387/3.382 Å ( $ls-1^{6+}/hs-1^{6+}$ ), while for the remaining oxo-anions the variation is less than 0.2 Å. The host charges also affect the hydrogen bonding dimensions, with a concomitant slight drop of the donor-acceptor N···O distances between incremental oxidation states, with the differences between the  $1^{3+}$  and  $1^{6+}$  being ca. 0.14 Å. Moreover, within a host's oxidation state, the hydrogen bonding and  $A_c \cdots N_3$  distances naturally reflect the  $V_{S,min}$  values of trigonal and tetrahedral oxo-anions.

The strength of the hydrogen bonding interactions between the host in  $1^{3+}$ ,  $1^{4+}$ ,  $1^{5+}$  and  $1^{6+}$  and each oxo-anion was ascertained through the Quantum Theory of Atoms in Molecules (QTAIM)<sup>[78,79]</sup> and by Natural Bond Orbital (NBO) analysis.<sup>[80,81]</sup> The QTAIM analysis revealed the existence of a bond critical point (BCP) between every N–H binding site and the anion's oxygen atoms involved in the three hydrogen bond interactions, as illustrated in Fig. S25 for  $CH_3COO^-$  or  $H_2PO_4^-$  hosted in the  $\alpha$ -binding pocket of  $1^{3+}$ . The electron density ( $\rho$ ), its Laplacian derivative ( $\nabla^2\rho$ ) and the potential energy density ( $\mathcal{V}$ ), all averaged from the calculated data at the three BCPs, are gathered in Table S9, together with the energy of the hydrogen bonds ( $E_{HB}$ ), estimated from  $\mathcal{V}$  as  $E_{HB} = \frac{1}{2}\mathcal{V}$ .<sup>[82]</sup>

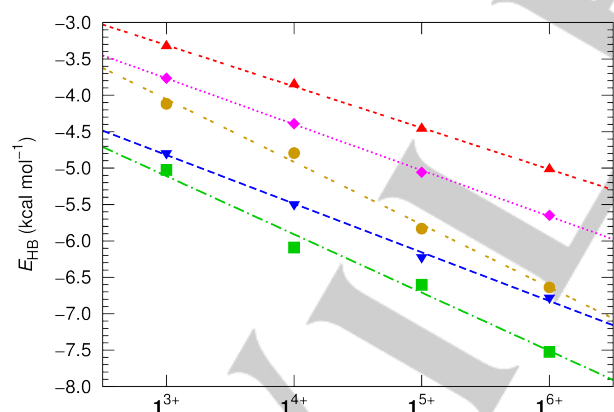


**Fig. 6** – Average  $E_{HB}$  energy values ( $\text{kcal mol}^{-1}$ ) for the hydrogen bonds between  $1^{n+}$  and  $CH_3COO^-$  (■),  $NO_3^-$  (●),  $ClO_4^-$  (▲),  $HSO_4^-$  (◆) or  $H_2PO_4^-$  (▼) as a function of  $1^{n+}$  oxidation state, together with their linear fits ( $R^2 \geq 0.984$ ). The values for high-spin electron configurations are not plotted, as the hydrogen bonds in both electron configurations have comparable  $E_{HB}$  energy values.

The  $\nabla^2\rho$  values are positive for all host-guest systems, indicating a depletion of the electron distribution consistent with the formation of the hydrogen bonding interactions. Moreover, the  $E_{HB}$  values for each hosted anion yield good linear relationships with

the host's oxidation states (see Fig. 6), indicating that the hydrogen bond strength increases with the host's net charge.

On the other hand, for each oxidation state of the host, the average  $E_{HB}$  values along the oxo-anion series (see Table S9) follow the same order  $CH_3COO^- > H_2PO_4^- > NO_3^- > HSO_4^- > ClO_4^-$ , indicating that the N–H···O hydrogen bonding interactions with the more basic acetate are the strongest, while the tetrahedral perchlorate, with lowest Lewis basicity, is the weakest bonded anion, in agreement with the oxo-anions'  $V_{S,min}$  trend (*vide supra*). For  $1^{3+}$ , this hydrogen bond strength trend is consistent with the  $^1\text{H-NMR}$  binding data (see Table 1), apart from  $HSO_4^-$ , that has the highest association constant.

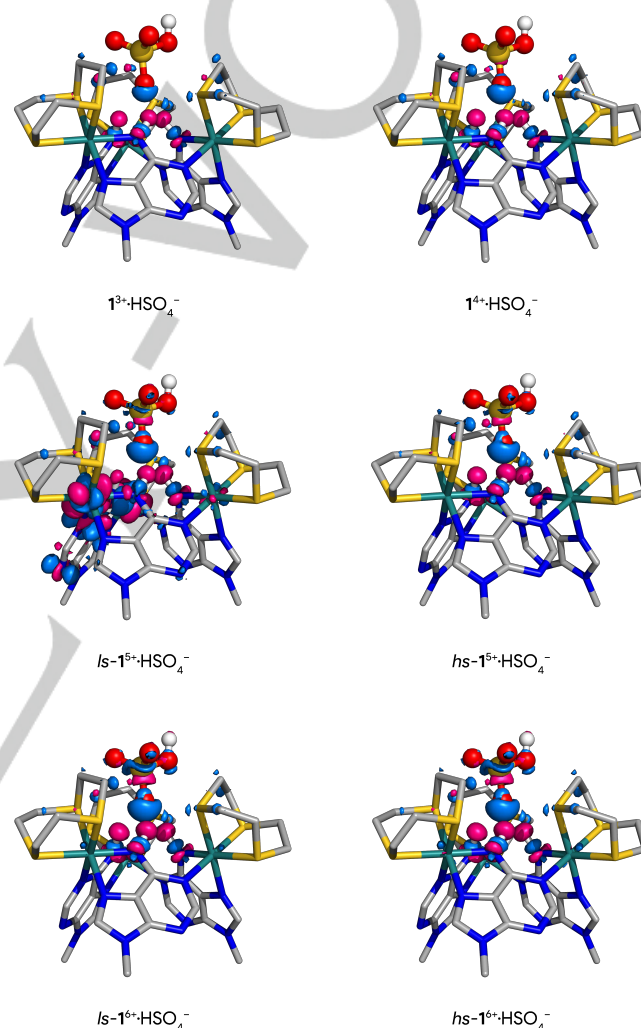


**Fig. 7** – Electron density difference ( $\Delta\rho = \rho[1^{n+}\cdot HSO_4^-] - \rho[1^{n+}] - \rho[HSO_4^-]$ , with  $n = 3-6$ ) maps for  $1^{n+}$  associated with  $HSO_4^-$ . Blue indicates increase of electron density ( $+0.002 \text{ ea}_0^{-3}$  contour) and magenta indicates loss of electron density ( $-0.002 \text{ ea}_0^{-3}$  contour).

In the NBO methods, a natural population analysis (NPA) indicates that anion binding is accompanied by a charge transfer from the anion to the host (see Fig. S26). In other words, anion binding occurs with progressive accumulation of electron density between the N–H binding sites and the hydrogen bonded anion oxygen atom, across the host oxidation states, as illustrated with the electron density difference maps for  $1^{n+}$  associated with  $HSO_4^-$  in Fig. 7 (remaining details in ESI).

As part of the NBO analysis, the three N–H···O hydrogen bonds were also evaluated as interactions between the electron lone pairs of an oxygen atom of the oxo-anion and the N–H antibonding orbitals of  $1^{n+}$ :  $n_O \rightarrow \sigma_{N-H}^*$ . The donor-acceptor stabilisation energies ( $E^2$ ), estimated by 2<sup>nd</sup>-order perturbation theory only for the three N–H···O hydrogen bonds between each oxo-anion and  $1^{n+}$  (see Table S10 and Fig. S27), reveal that these synergetic interactions are also largely dependent of the host oxidation state, mirroring the linear tendencies previously obtained with  $E_{HB}$  calculated from  $\mathcal{V}$  values (*vide supra*),  $\Delta H_{HG}$  and  $\Delta G_{HG}^{SS}$ .

In summary, the three quantum descriptors,  $\Delta H_{HG}$ ,  $E_{HB}$ , and  $E^2$  show that the binding affinity of  $1^{n+}$  towards the oxo-anions is mainly dictated by the N–H···O charge-assisted hydrogen bonding interactions. In line with this outcome, when the logarithms of the association constants (Table 2) estimated for tetragonal ( $\text{ClO}_4^-$ ) and trigonal ( $\text{NO}_3^-$ ) anions are plotted against the values of  $\Delta H_{HG}$ ,  $E_{HB}$ , or  $E^2$  highly linear relationships are observed (Fig. 8,  $R^2 \geq 0.892$ ).

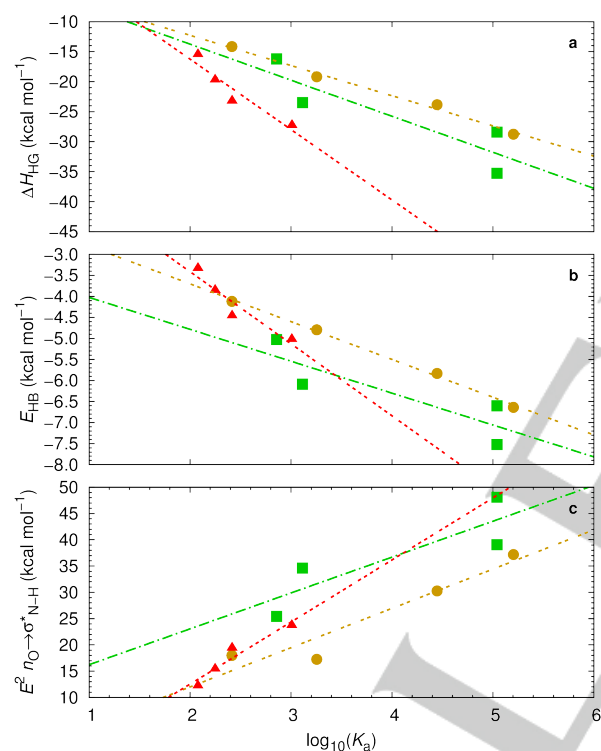


**Fig. 8** – Quantum parameters as a function of  $\log_{10}(K_a)$  for the anion associations of  $1^{n+}$  and  $\text{CH}_3\text{COO}^-$  (■),  $\text{NO}_3^-$  (●),  $\text{ClO}_4^-$  (▲), together with the corresponding linear fits: **a** Variation of the  $\Delta H_{HG}$  ( $\text{kcal mol}^{-1}$ ) between  $1^{n+}$  and the oxo-anion ( $R^2 \geq 0.793$ ); **b** Average  $E_{HB}$  energy values ( $\text{kcal mol}^{-1}$ ) for the hydrogen bonds between  $1^{n+}$  and the oxo-anion ( $R^2 \geq 0.753$ ); **c** Variation of the  $E^2$  stabilisation energies of  $n_O \rightarrow \sigma_{N-H}^*$  ( $\text{kcal mol}^{-1}$ ) for the N–H···O interactions ( $R^2 \geq 0.741$ ). The points for the high-spin electron configurations are not plotted as they would overlap with the low-spin configurations data.

**Halide anion binding reanalysis** Within the comprehensive assessment of the binding properties of  $1^{n+}$  for a wide range of anions, our previous theoretical studies on halide associations were also revisited. The calculations previously performed for  $1^{3+}$  were extended to the remaining host's oxidation states, using the same level of theory applied to the polyatomic anion associations. Moreover, following our previous calculations on the halide

associations of  $1^{3+}$ , the mono-atomic anions were described with the aug-cc-pVDZ ( $\text{F}^-$  and  $\text{Cl}^-$ ) or aug-cc-pVDZ-PP ( $\text{Br}^-$  and  $\text{I}^-$ ) basis sets. Likewise for the polyatomic anions, two binding scenarios with the halides hosted in the  $\alpha$  or  $\beta$  pockets of  $1^{n+}$  were evaluated. The optimised structures obtained in these two alternative binding arrangements are shown in Figs. S28–S35, while the computed distances between halides and the  $\text{N}_3$  plane of  $1^{n+}$  (*vide supra*) are collected in Table S11 for the host-guest associations with the anion in the  $\alpha$  and  $\beta$  pockets, respectively. The  $\Delta H_{HG}$  values summarised in Table S12 indicate that all halides have a strong binding preference for the  $\alpha$  pocket, with the energetic gap between the two alternative binding arrangements increasing linearly with the host's oxidation state for the four anions (see Fig. S36, all  $R^2 \geq 0.938$ ). This is particularly evident for  $\text{F}^-$  associations with enthalpy differences between the  $\alpha$  and  $\beta$  pockets ranging from  $-15.5 \text{ kcal mol}^{-1}$  for  $1^{3+}$  to ca.  $-30.1 \text{ kcal mol}^{-1}$  for  $1s\text{-}1^{6+}/hs\text{-}1^{6+}$ .

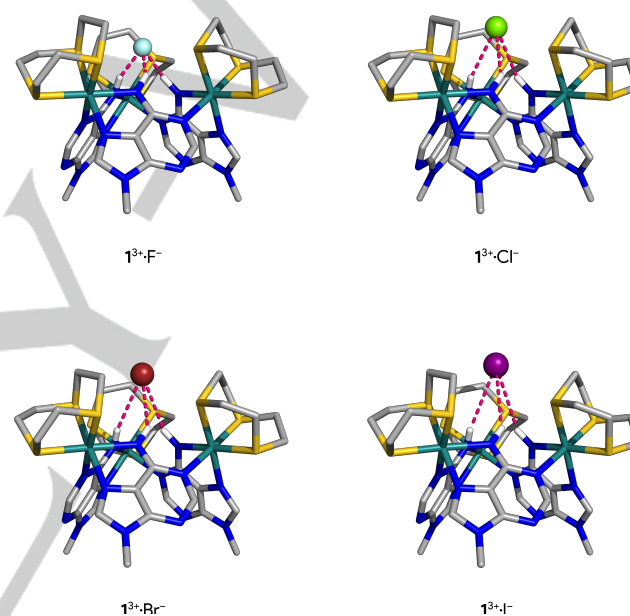


**Fig. 9.** DFT optimised structures of  $1^{3+}$  halide associations in the  $\alpha$  pocket. The N–H···X (X =  $\text{F}^-$ ,  $\text{Cl}^-$ ,  $\text{Br}^-$  or  $\text{I}^-$ ) hydrogen bonds are drawn as pink dashed lines. The C–H hydrogen atoms were hidden for clarity.

In the DFT optimised structures, the N–H binding sites of the  $1^{n+}$  hosts establish with each halide (X =  $\text{F}^-$ ,  $\text{Cl}^-$ ,  $\text{Br}^-$  or  $\text{I}^-$ ) three convergent hydrogen bonds with geometric parameters listed in Table S13. Irrespective to the host oxidation state, the average hydrogen bond donor-acceptor distances ( $\text{N}\cdots\text{X}$ ), increase through the halide series, together with the  $\text{X}\cdots\text{N}_3$  ones, mainly mirroring the anions' volume and  $V_{S,\text{min}}$  values (in  $\text{kcal mol}^{-1}$ ) trends, as follows:  $\text{I}^- (-123.8) > \text{Br}^- (-133.6) > \text{Cl}^- (-141.0) > \text{F}^- (-171.0)$ . For instance, the smallest  $\text{F}^-$  anion is tightly hydrogen bonded to  $1^{3+}$  and deeply inserted into the  $\alpha$  pocket, with average  $\text{N}\cdots\text{X}$  and  $\text{X}\cdots\text{N}_3$  distances of 2.764 and 2.122 Å, respectively, while the bulkiest  $\text{I}^-$  with average  $\text{N}\cdots\text{X}$  distances of 4.147 Å hovers just above the crown methylene bridges at an  $\text{X}\cdots\text{N}_3$  distance of 3.736 Å. The relative positions occupied by the monoatomic anions in the  $\alpha$  pocket of  $1^{n+}$  are illustrated in Fig. 9 with the  $1^{3+}$  host-guest complexes.

These new theoretical structural data contrast with the data previously obtained from DFT geometry optimisations carried out

for the  $1^{3+}$  halide complexes using the same DFT functional but without the dispersion corrections, coupled with the lower 6-31G(d) basis set for C, N, H and S centres, which was dictated by the limited computing power available at that time. While the computed structure for the  $\text{Cl}^-$  complex shows comparable hydrogen bonds dimensions, the interactions of the remaining halides with the host's  $\alpha$  pocket were characterised by much higher intermolecular  $\text{N}\cdots\text{X}$  distances than those reported here.

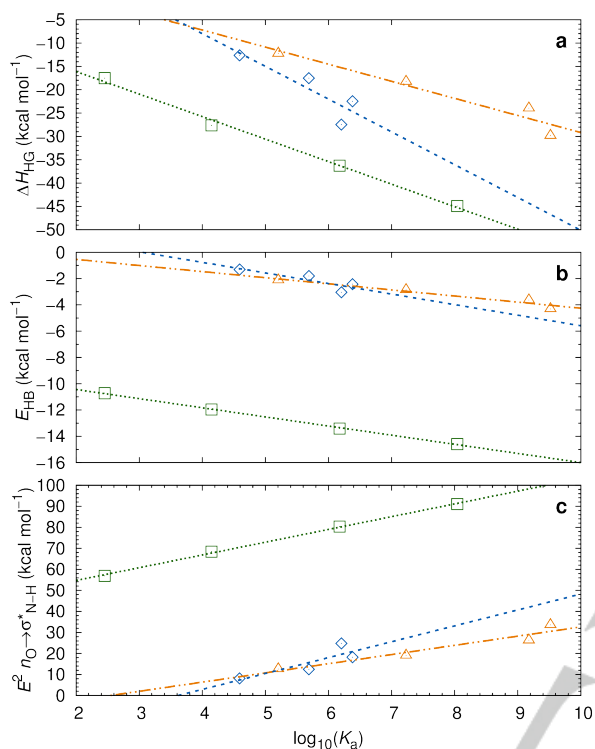


**Fig. 10.** Quantum parameters as a function of  $\log_{10}(K_a)$  for the anion associations of  $1^{n+}$  and  $\text{F}^-$  ( $\square$ ),  $\text{Cl}^-$  ( $\triangle$ ) and  $\text{Br}^-$  ( $\diamond$ ), together with the corresponding linear fits: **a** Variation of the  $\Delta H_{\text{HG}}$  ( $\text{kcal mol}^{-1}$ ) between  $1^{n+}$  and the oxo-anion ( $R^2 \geq 0.781$ ); **b** Average  $E_{\text{HB}}$  energy values ( $\text{kcal mol}^{-1}$ ) for the hydrogen bonds between  $1^{n+}$  and the oxo-anion ( $R^2 \geq 0.746$ ); **c** Variation of the  $E^2$  stabilisation energies of  $n_{\text{X}} \rightarrow \sigma_{\text{N-H}}^*$  ( $\text{kcal mol}^{-1}$ ,  $\text{X} = \text{F}^-, \text{Cl}^-, \text{Br}^-$  or  $\text{I}^-$ ) for the  $\text{N-H}\cdots\text{O}$  interactions ( $R^2 \geq 0.710$ ). The points for the high-spin electron configurations are not plotted as they would overlap with the low-spin configurations data.

As observed for the polyatomic anion host-guest complexes, the average  $\text{N}\cdots\text{X}$  and  $\text{X}\cdots\text{N}_3$  distances progressively decrease along the host's oxidation states, suggesting that the host's net charge enhances the strength of the host-guest hydrogen bonding, as demonstrated by the following energetic analysis.

The computed binding data, summarised in Table S12, show that the binding interaction between halides and the  $\alpha$  pocket of  $1^{n+}$  is thermodynamically favourable, with the binding free energies being mainly determined by the enthalpic term, while the  $T\Delta S$  contribution is comparable for all halide host-guest associations and host's oxidation states. The theoretical  $\Delta H_{\text{HG}}$  values lead to the binding affinity order  $\text{F}^- > \text{Cl}^- \approx \text{Br}^- \approx \text{I}^-$  for  $1^{3+}$ ,  $\text{F}^- > \text{Cl}^- \approx \text{Br}^- > \text{I}^-$  for  $1^{4+}$  and  $\text{F}^- > \text{Cl}^- > \text{Br}^- > \text{I}^-$  for the subsequent host's oxidation states, whereas the corresponding  $\Delta G_{\text{HG}}^{\text{SS}}$  values yield a well-defined binding trend  $\text{F}^- > \text{Cl}^- > \text{Br}^- > \text{I}^-$ , which is corroborated when the  $E_{\text{HB}}$  and  $E^2$  quantum descriptors are used to measure the strength of the  $\text{N-H}\cdots\text{X}$  hydrogen bonds (see Tables S14 and

S15). While the binding affinities predicted by these two energetic descriptors for host-guest complexes between  $\text{Cl}^-$ ,  $\text{Br}^-$  and  $\text{I}^-$  and  $1^{3+}$  are in line with experimental data, the superior binding affinity theoretically predicted for  $\text{F}^-$  is inconsistent with the lower binding affinity calculated from the experimental data for this oxidation state, which displays an association constant one order of magnitude smaller than for  $\text{I}^-$ .<sup>[58]</sup> However, in these calculations the MeCN solvent is treated using a polarized continuous solvent model (PCM). Acetonitrile is polar and hydrogen bonding, and is known to be a good solvent for fluoride.<sup>[83]</sup> As such, it will interact particularly strongly with the small, charge dense  $\text{F}^-$ , as apparent from its higher experimental solvation free energy in this solvent, when compared with the remaining halides:  $\text{F}^-$  (-88.0),  $\text{Cl}^-$  (-64.5),  $\text{Br}^-$  (-61.1), and  $\text{I}^-$  (-55.9  $\text{kcal mol}^{-1}$ ).<sup>[84]</sup> Therefore, it seems likely that the mismatch between computed and experimental thermodynamic data is due to the interaction of the macrocyclic host and a MeCN solvated fluoride anion rather than a "bare" anion. Indeed, it is well known that this effect is observed in host-guest experiments conducted in water.<sup>[85–87]</sup> Unfortunately, the explicit inclusion of MeCN solvent molecules into our DFT calculations is computationally prohibited due to the concomitant increase in complexity in already highly demanding calculations on the interaction between the multinuclear-metallomacrocyclic-based host and its guest.

On the other hand, Fig. S37 shows that for each halide, the values of  $\Delta H_{\text{HG}}$ ,  $E_{\text{HB}}$ , and  $E^2$  follow near perfect linear relationships with the progressive increasing of the host's oxidation state (all  $R^2 \geq 0.988$ ), while Fig. 10 shows that good fittings are obtained when these quantum binding descriptors are plotted against the logarithm values of the association constants calculated with experimental data for  $\text{F}^-$ ,  $\text{Cl}^-$  and  $\text{Br}^-$  ( $R^2 \geq 0.710$ ). These theoretical findings definitively indicate that the hydrogen bonding between halides and  $1^{n+}$  is charge assisted, as found for the oxo-anion complexes.

Upon binding of each halide by  $1^{n+}$ , a charge transfer occurs from the anion to the host, as illustrated in Fig. S38, where the net charge difference between the bound and free anion, obtained from the NPA analysis, is plotted against the oxidation state of  $1^{n+}$ .

In line with the results for the oxo-anions complexes, the charge transfer increases with the successive increase in host oxidation states, following linear relationships for each halide ( $R^2 \geq 0.993$ ), which also results in the accumulation of electron density between the  $\text{N-H}$  binding sites and the hydrogen bonded anion. This trend is illustrated in Fig. 11, which shows the electron density difference maps for  $1^{n+}$  associated with  $\text{Cl}^-$ .

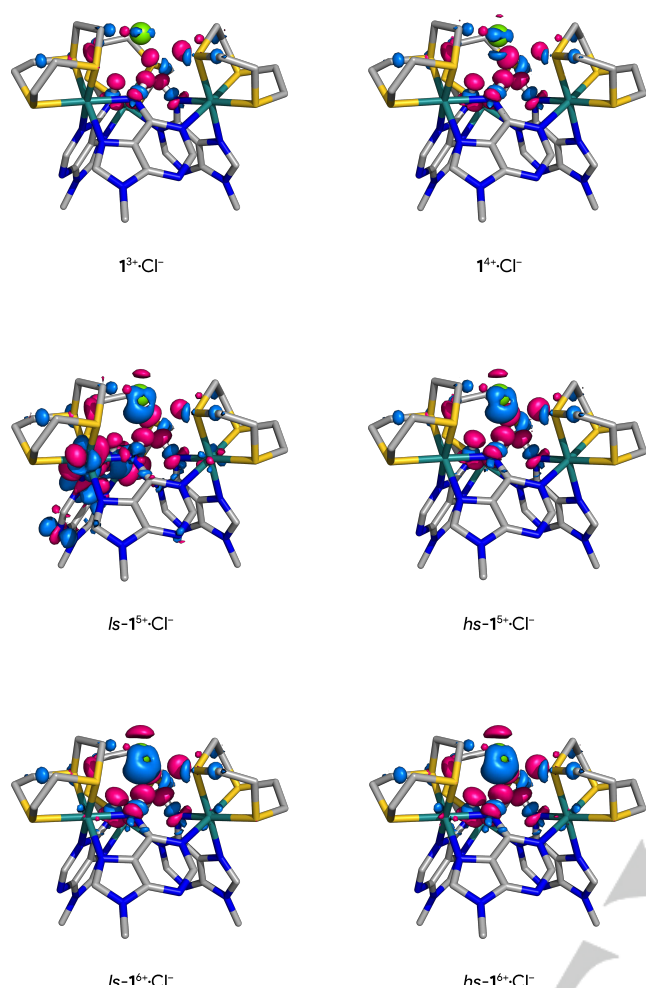


**Fig. 11.** Electron density difference ( $\Delta\rho = \rho[1^{n+}\cdot\text{Cl}^-] - \rho[1^{n+}] - \rho[\text{Cl}^-]$ , with  $n = 3-6$ ) maps for  $1^{n+}$  associated with  $\text{Cl}^-$ . Blue indicates increase of electron density ( $+0.002 e a_0^{-3}$  contour) and magenta indicates loss of electron density ( $-0.002 e a_0^{-3}$  contour).

**Correlation with electrochemical studies.** Further insights into electrochemistry behaviour of the  $1^{n+}$  host were obtained with the analysis of the highest-energy occupied molecular orbitals (HOMO) in free  $1^{n+}$  and in their oxo-anion associations. The main contribution to this frontier molecular orbital is from the three 9MA bridging ligands (see Fig. S39) in the presence or in absence of an anionic guest. The HOMO energy values, given in Table S16, as expected, lower with increasing host oxidation state. On the other hand, the anion binding in the  $\alpha$  pocket only slightly raises the energy of the HOMO in all oxidation states, in agreement with their negligible contributions to this orbital. The ionisation potentials (IP) of  $1^{n+}$ , both free and anion associated, were roughly estimated from the HOMO energies, using Koopman's theorem ( $IP_K = -E_{\text{HOMO}}$ ),<sup>[88]</sup> as well as through the more accurate adiabatic approach,<sup>[89]</sup> using the differences between the absolute electronic energies of the optimised structures in consecutive oxidation states ( $IP_A = \mathcal{E}_0^{(n+1)+} - \mathcal{E}_0^{n+}$ , with  $n$  ranging from 3 to 5). The  $IP_A$  values are gathered in Table S17 together with the  $IP_K$  ones. Overall, the IP values indicate that the energy required to remove an electron increases with the oxidation state of  $1^{n+}$ . Moreover, the hosted anions facilitate the successive oxidation of  $1^{3+}$ , in agreement with the electrochemical data. Furthermore, mirroring the  $\Delta H_{\text{HG}}$  interaction energies, the tightly bonded  $\text{H}_2\text{PO}_4^-$

more easily enables successive electron loss. The same insight arises from the overestimated  $IP_K$  values.

The interactions between halides and  $1^{n+}$  raise the HOMO energies of the host-guest complexes relatively to the free hosts (Table S16), facilitating the successive oxidation of  $1^{3+}$ , as indicated by the ionisation potentials estimated either using Koopman's or the adiabatic approach (*vide supra*). The  $IP_K$  and  $IP_A$  values for free  $1^{n+}$  and their halide associations are listed in Table S17. Overall, the ionisation potentials for the  $\text{Cl}^-$  and  $\text{Br}^-$  associations are comparable with those for the  $\text{CH}_3\text{COO}^-$ ,  $\text{NO}_3^-$ ,  $\text{HSO}_4^-$  and  $\text{H}_2\text{PO}_4^-$  associations, hinting at their potential to successively oxidise  $1^{n+}$ . On the other hand, the low affinity guests  $\text{I}^-$  and  $\text{ClO}_4^-$  appear to be equally ineffective in facilitating the successive oxidation of  $1^{n+}$ . Therefore, this comparison shows that the anion binding strength and the hosted anion's ability to promote the successive oxidation of  $1^{n+}$  host are straightforward related.

**Interaction with the hexafluorophosphate anion.** The crystal structure of  $1^{3+}$  with  $\text{PF}_6^-$  inspired us to evaluate the host-guest interactions between this ion-pair using the theoretical approach devised for the oxo-anions and the halide series. The DFT computed structure for the  $1^{3+}\cdot\text{PF}_6^-$  stoichiometry with the octahedral anion lodged in the  $\alpha$  pocket (see Fig. 12, left panel), has the centre of mass of this anionic guest, the phosphorous atom, only 4.048 Å away from the  $\text{N}_3$  equatorial plane (*vide supra*), while in the X-ray crystal structure the anion is at a longer  $\text{P}\cdots\text{N}_3$  distance of 4.504 Å. Three fluorine atoms establish three single  $\text{N}\cdots\text{H}\cdots\text{F}$  hydrogen bonds to  $1^{3+}$ , with an average donor-acceptor  $\text{N}\cdots\text{F}$  distance of  $3.14 \pm 0.01$  Å, which is markedly shorter (*ca.* 0.5 Å) than those observed in the X-ray structure (see Table S18). On the other hand, in the  $\beta$  pocket (see Fig. 12, right panel),  $\text{PF}_6^-$  is also more deeply embedded in the computed model than in the solid-state structure, with  $\text{P}\cdots\text{N}_3$  distances of 5.128 and 5.986 Å, respectively (Table S18). Overall, these two alternative binding arrangements are preserved along the remaining three oxidation states (see Figs. S40 and S41), accompanied by inherent shortening of the  $\text{P}\cdots\text{N}_3$  distances and increase of the  $\text{N}\cdots\text{H}\cdots\text{F}$  hydrogen bonds' strength, as evident from the dimensions of these two structural parameters gathered in Table S18.

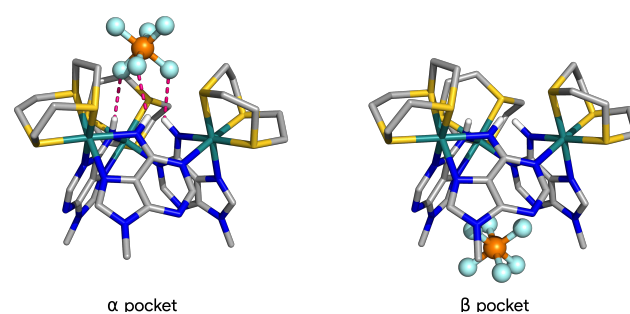


**Fig. 12.** DFT optimised structures of  $1^{3+}$  associations with octahedral anion  $\text{PF}_6^-$  in the  $\alpha$  or  $\beta$  pockets. The  $\text{N}\cdots\text{H}\cdots\text{F}$  hydrogen bonds are drawn as pink dashed lines. The  $\text{C}\cdots\text{H}$  hydrogen atoms were hidden for clarity.

In agreement with  $\text{PF}_6^-$  weak binding ability, the estimated  $\Delta H_{\text{HG}}$  (see Table S19),  $E_{\text{HB}}$ , and  $E^2$  values for the anion's interaction with  $\alpha$  pocket of  $1^{n+}$  (summarised in Table S20) are lower than those obtained for the oxo-anions and halides but follow equivalent energetic trends with the host's oxidation state (see Fig. S42). However, the enthalpy yielded with hydrogen bonding interactions

between  $\text{PF}_6^-$  and  $1^{3+}$  of  $-11.1 \text{ kcal mol}^{-1}$  is overwhelmed by the  $-T\Delta S$  entropic penalty of  $13.6 \text{ kcal mol}^{-1}$ , leading to a slightly unfavourable binding free energy ( $\Delta G_{\text{HG}}$ ) of ca.  $2.4 \text{ kcal mol}^{-1}$ , in spite of the hydrogen bonding dimensions in the calculated structure being shorter than those found in the solid-state (*vide supra*). The formation of  $\text{PF}_6^-$  hydrogen bond associations with  $1^{n+}$  host in the subsequent oxidation states are thermodynamically favourable, being determined by enthalpy. On the other hand, the  $\Delta\Delta H_{\text{HG}\alpha-\beta}$  values plotted in Fig. S43, show that the binding preference of  $\text{PF}_6^-$  for the  $\alpha$  pocket of  $1^{n+}$  diminishes with the increase of the host's oxidation state. Indeed, while  $\text{PF}_6^-$ , with a volume<sup>REFA1</sup> of  $97.72 \text{ \AA}^3$  and a  $V_{\text{S,min}}$  of  $-118.4 \text{ kcal mol}^{-1}$ , prefers the  $\alpha$  pocket of  $1^{4+}$  by an  $\Delta\Delta H_{\text{HG}\alpha-\beta}$  value of  $-1.3 \text{ kcal mol}^{-1}$ , in the last two oxidation states, independently of the host's spin multiplicities, the recognition of the octahedral anion is likely in either the  $\alpha$  or  $\beta$  pocket, with the latter one being slightly favoured by an enthalpy of ca.  $0.1$  and  $0.7 \text{ kcal mol}^{-1}$  in  $1^{5+}$  and  $1^{6+}$ , respectively. This progressive loss of the binding preference for the  $\alpha$  pocket across the four oxidation states should be related with the increasing role of the non-covalent interactions between  $\text{PF}_6^-$  and the  $\pi$ -electron-deficient 9MA bridging ligands of the  $\beta$  pocket, within the electrostatic regime of attractive intermolecular forces. Indeed, while the QTAIM analysis of the optimised  $\alpha$  pocket  $1^{n+}\cdot\text{PF}_6^-$  associations reveals three BCPs derived from the N-H $\cdots$ F hydrogen bonding interactions, the computed structures for the  $\beta$  pocket associations show two BCPs between the fluorine atoms and each 9MA aromatic bridging face (amounting to 6 BCPs), attributed to anion- $\pi$  interactions with the bowl cavity, as illustrated in Fig. S44.

The theoretical calculations in MeCN implicit solvent indicate that the recognition of the hydrophobic  $\text{PF}_6^-$  anion by  $1^{3+}$  is disfavoured in either binding cavity, with  $\Delta G^{\text{SS}}_{\text{HG}}$  values of  $0.6$  and  $3.9 \text{ kcal mol}^{-1}$  for the  $\alpha$  and  $\beta$  pockets, respectively. On the other hand, the solid-state structure between  $1^{3+}$  and  $\text{PF}_6^-$  suggests the existence of a supramolecular association with a 1:2 host-guest stoichiometry. These results also lead us to investigate this association by DFT calculations. In the computed structure (see Fig. S45), the two  $\text{PF}_6^-$  are separated by a P $\cdots$ P distance of  $9.458 \text{ \AA}$ , with the anions hosted in  $\alpha$  and  $\beta$  pockets positioned at P $\cdots$ N<sub>3</sub> distances (*vide supra*) of  $4.078$  and  $5.379 \text{ \AA}$ , respectively. While the former P $\cdots$ N<sub>3</sub> distance is identical to the one determined for the 1:1 stoichiometry, with  $\text{PF}_6^-$  hydrogen bonded to the 9MA bridging ligands, the later P $\cdots$ N<sub>3</sub> distance, for the  $\text{PF}_6^-$  interacting with  $\beta$  pocket through weak anion- $\pi$  interactions, has an intermediate value between the distance computed for the 1:1 stoichiometry and the one observed in the crystal structure, reflecting the reduction of the ion-ion interactions derived from the presence of a  $\text{PF}_6^-$  anion in the  $\alpha$  pocket. However, the formation of the  $1^{3+}\cdot(\text{PF}_6^-)_2$  association in MeCN media is disfavoured by a free energy penalty of  $7.9 \text{ kcal mol}^{-1}$ , suggesting that the intermolecular interactions found in the crystal structure of  $1^{3+}$  and  $\text{PF}_6^-$  should be assigned to packing effects.

## Conclusion

A comparison of experimental binding data for the different oxidation states of self-assembled host  $1^{n+}$  with oxo and halide anions shows a  $>10^7$  range of binding affinities, with the highest values observed for the  $\text{Cl}^-$  ion guest in the host's isovalent  $\text{Ru}^{\text{III}}$  oxidation state. The experimental evidence from these binding

studies points to an important contribution from electrostatically enhanced hydrogen-bonding. Yet, apart from binding to  $\text{F}^-$  – which shows a simple linear relationship with the increasing charge of the host – recognition of larger and more structurally complex anions clearly involves other factors, such as non-covalent interactions between  $1^{n+}$  and MeCN solvent molecules (e.g., putative hydrogen bonds and dispersion forces), which were not considered in our computational studies, as they were carried out using an implicit solvent model. It is also notable that in both the halide and oxo-anion series, the anion that produces the poorest agreement between experimental and computational results – fluoride and acetate respectively – is highest within the Hoffmeister series.<sup>[90]</sup> These observations indicate that, just as in water, the solvation effects of the polar, hydrogen bonding MeCN<sup>[87]</sup> likely play a significant role in the decreased correlation observed for these anions.

Nevertheless, in agreement with the experimental data, the DFT calculations indicate that  $1^{n+}$ , in its four oxidation states, hosts the oxo-anions into the  $\alpha$  pocket through three synergetic hydrogen bonding interactions. The oxo-anion guests binding preference for the  $\alpha$  pocket is independent of the oxidation state and spin multiplicity of this trinuclear macrocyclic receptor. The QTAIM and NBO analyses show that throughout the successive oxidation states of  $1^{n+}$ , the strength of the charge assisted hydrogen bonds increases, leading to a progressive growth of the charge transfer from the oxo-anions and halides to the metallo-macrocyclic host and its consequent stabilization. A fuller understanding of the complex interplay of multiple effects which drives the entropy-enthalpy compensation effects observed in these studies will require further comprehensive, temperature-dependent, thermodynamics studies. Such work will provide a dialogue with the theoretical studies discussed herein and offer data for further insights and development of these models. Such experiments and their accompanying theoretical studies will form the basis of subsequent reports.

Moreover, while the energy binding data indicate that the recognition of the octahedral  $\text{PF}_6^-$  anion in  $1^{4+}$  oxidation state mainly occurs in the  $\alpha$  pocket, in the two subsequent oxidation states the recognition can occur in either pocket, due to the putative enhancement of the anion- $\pi$  interactions.

The experimental observations and computational studies chime with recent studies showing that anion recognition by conventionally synthesised macrocyclic receptors such as calixpyroles, triazolophanes, and cyanostars operate “beyond the electrostatic regime” and require a consideration of more subtle interactions such as induced dipoles and dispersion forces.<sup>[91,92]</sup> With our multi-redox-state receptor a further factor becomes apparent. A comparison of the interaction of  $1^{5+}$  and  $1^{6+}$  with acetate reveals that this panoply of host-guest interactions and steric factors can thermodynamically stabilize the receptor in a specific oxidation state leading to binding affinities that are unchanged even after an appreciable increase in the electrostatic contribution to binding.

As illustrated by its electrochemical properties, unlike related systems<sup>[93–95]</sup> receptor  $1^{3+}$  is kinetically inert, suggesting that it can be used for analogous studies in water where hydrophobic interactions will contribute to and modulate guest recognition phenomenon. Furthermore, through the judicious selection of appropriate building blocks, higher order macrocyclic structures that provide access to a wider range of redox states can also be

envisaged. Such studies are underway and will form the basis of future reports.

## Experimental Section

Complex [1](PF<sub>6</sub>)<sub>3</sub> was synthesized by a reported route.<sup>[56]</sup>

## Acknowledgements

The computational studies were funded within the scope of the project CICECO-Aveiro Institute of Materials, UIDP/50011/2020, financed by national funds through the Portuguese Foundation for Science and Technology/MCTES. A.Z. is grateful to the Libyan government financial support through a PhD studentship. HAA is grateful for a PhD scholarship provided by the Ministry of Education, Kingdom of Saudi Arabia. We are grateful to the reviewers whose comments and suggestions on this report have substantially improved its quality.

**Keywords:** Ruthenium; Self-assembly; anion-recognition; electrochemistry; DFT.

- [1] P. D. Beer, P. a. Gale, *Angew. Chem. Int. Ed. Engl.* **2001**, *40*, 486–516.
- [2] R. Martínez-Máñez, F. Sancenón, *Chem. Rev.* **2003**, *103*, 4419–4476.
- [3] A. E. Hargrove, S. Nieto, T. Zhang, J. L. Sessler, E. V Anslyn, *Chem. Rev.* **2011**, *111*, 6603–6782.
- [4] N. H. Evans, P. D. Beer, *Angew. Chemie Int. Ed.* **2014**, *53*, 11716–11754.
- [5] M. J. Langton, C. J. Serpell, P. D. Beer, *Angew. Chemie - Int. Ed.* **2016**, *55*, 1974–1987.
- [6] J. L. Sessler, S. Camiolo, P. a Gale, *Coord. Chem. Rev.* **2003**, *240*, 17–55.
- [7] Y. Li, A. H. Flood, *J. Am. Chem. Soc.* **2008**, *130*, 12111–12122.
- [8] P. Ballester, *Acc. Chem. Res.* **2013**, *46*, 874–884.
- [9] S. Lee, C.-H. Chen, A. H. Flood, *Nat. Chem.* **2013**, *5*, 704–710.
- [10] M. A. Yawer, V. Havel, V. Sindelar, *Angew. Chemie Int. Ed. English* **2014**, *54*, 276–279.
- [11] K.-C. Chang, T. Minami, P. Koutnik, P. Y. Savechenkov, Y. Liu, P. Anzenbacher Jr., *J. Am. Chem. Soc.* **2014**, *136*, 1520–1525.
- [12] P. A. Gale, E. N. W. Howe, X. Wu, *Chem. - A Eur. J.* **2016**, *1*, 351–422.
- [13] N. Busschaert, C. Caltagirone, W. Van Rossom, P. A. Gale, *Chem. Rev.* **2015**, *115*, 8038–8155.
- [14] S. Kubik, *Chem. Soc. Rev.* **2010**, *39*, 3648–3663.
- [15] J. Zhao, D. Yang, X.-J. Yang, B. Wu, *Coord. Chem. Rev.* **2019**, *378*, 415–444.
- [16] E. Graf, J.-M. Lehn, *J. Am. Chem. Soc.* **1976**, *98*, 6403–6405.
- [17] S. Otto, S. Kubik, *J. Am. Chem. Soc.* **2003**, *125*, 7804–7805.
- [18] H. T. Chifotides, I. D. Giles, K. R. Dunbar, *J. Am. Chem. Soc.* **2013**, *135*, 3039–3055.
- [19] S. T. Schneebeli, M. Frascioni, Z. Liu, Y. Wu, D. M. Gardner, N. L. Strutt, C. Cheng, R. Carmieli, M. R. Wasielewski, J. F. Stoddart, *Angew. Chemie Int. Ed. English* **2013**, *52*, 13100–13104.
- [20] P. Molina, F. Zapata, A. Caballero, *Chem. Rev.* **2017**, *117*, 9907–9972.
- [21] Y. Lei, L. Shen, J.-R. Liu, T. Jiao, Y. Zhang, C. Zhang, L. Tong, X. Hong, Y. Pan, H. Li, *Chem. Commun.* **2019**, *55*, 8297–8300.
- [22] Y. Liu, W. Zhao, C.-H. Chen, A. H. Flood, *Science (80- )*. **2019**, *365*, 159–161.
- [23] M. H. Keefe, K. D. Benkstein, J. T. Hupp, *Coord. Chem. Rev.* **2000**, *205*, 201–228.
- [24] Z. Liu, W. He, Z. Guo, *Chem. Soc. Rev.* **2013**, *42*, 1533–1568.
- [25] M. H. Lee, J. S. Kim, J. L. Sessler, *Chem. Soc. Rev.* **2015**, *44*, 4185–4191.
- [26] L. You, D. Zha, E. V Anslyn, *Chem. Rev.* **2015**, *115*, 7840–7892.
- [27] G.-L. Wang, Y.-J. Lin, G.-X. Jin, *Chem. - A Eur. J.* **2011**, *17*, 5578–5587.
- [28] I. A. Riddell, M. M. J. Smulders, J. K. Clegg, Y. R. Hristova, B. Breiner, J. D. Thoburn, J. R. Nitschke, *Nat. Chem.* **2012**, *4*, 751–756.
- [29] A. Mishra, V. Vajpayee, H. Kim, M. H. Lee, H. Jung, M. Wang, P. J. Stang, K.-W. Chi, *Dalt. Trans.* **2012**, *41*, 1195–1201.
- [30] T. K. Ronson, S. Zarra, S. P. Black, J. R. Nitschke, *Chem. Commun.* **2013**, *49*, 2416–2476.
- [31] R. Dutta, P. Ghosh, *Chem. Commun.* **2014**, *50*, 10538–10554.
- [32] D. P. August, G. S. Nichol, P. J. Lusby, *Angew. Chemie Int. Ed. English* **2016**, *55*, 15022–15026.
- [33] C. R. Rice, C. Slater, R. A. Faulkner, R. L. Allan, *Angew. Chemie Int. Ed. English* **2018**, *57*, 13071–13075.
- [34] W. Zhang, D. Yang, J. Zhao, L. Hou, J. L. Sessler, X.-J. Yang, B. Wu, *J. Am. Chem. Soc.* **2018**, *140*, 5248–5256.
- [35] C. Creutz, H. Taube, *J. Am. Chem. Soc.* **1969**, *91*, 3988–3989.
- [36] D. E. Richardson, H. Taube, *Coord. Chem. Rev.* **1984**, *60*, 107–129.
- [37] W. Kaim, A. Klein, M. Glöckle, *Acc. Chem. Res.* **2000**, *33*, 755–763.
- [38] K. D. Demadis, C. M. Hartshorn, T. J. Meyer, *Chem. Rev.* **2001**, *101*, 2655–2686.
- [39] W. Kaim, B. Sarkar, *Coord. Chem. Rev.* **2007**, *251*, 584–594.
- [40] W. Kaim, G. K. Lahiri, *Angew. Chem. Int. Ed. Engl.* **2007**, *46*, 1778–96.
- [41] J. A. Thomas, *Coord. Chem. Rev.* **2013**, *257*, 1555–1563.
- [42] M. D. Ward, *Chem. Soc. Rev.* **1995**, *24*, 121–134.
- [43] F. Paul, C. Lapinte, *Coord. Chem. Rev.* **1998**, *178*, 431–509.
- [44] A. Harriman, R. Ziessel, *Coord. Chem. Rev.* **1998**, *171*, 331–339.
- [45] J. P. Launay, *Chem. Soc. Rev.* **2001**, *30*, 386–397.
- [46] O. S. Wenger, *Chem. Soc. Rev.* **2012**, *41*, 3772–3779.
- [47] B. Sarkar, D. Schweinfurth, N. Deibel, F. Weisser, *Coord. Chem. Rev.* **2015**, *293–294*, 250–262.
- [48] M. B. Robin, P. Day, in *Adv Inorg Chem Radiochem* (Eds.: H.J. Emeléus, Sharpe), Elsevier, **1968**, pp. 247–422.
- [49] P. de Wolf, P. Waywell, M. Hanson, S. L. Heath, A. J. H. M. Meijer, S. J. Teat, J. A. Thomas, *Chem. - A Eur. J.* **2006**, *12*, 2188–2195.
- [50] H. Ahmad, B. W. Hazel, A. J. H. M. Meijer, J. A. Thomas, K. A. Wilkinson, *Chem. - A Eur. J.* **2013**, *19*, 5081–5087.
- [51] C. Metcalfe, H. Adams, I. Haq, J. A. Thomas, *Chem. Commun.* **2003**, 1152–1153.
- [52] C. Rajput, R. Rutkaite, L. Swanson, I. Haq, J. a Thomas, *Chemistry* **2006**, *12*, 4611–9.
- [53] S. P. Foxon, T. Phillips, M. R. Gill, M. Towrie, A. W. Parker, M. Webb, J. a Thomas, *Angew. Chem. Int. Ed. Engl.* **2007**, *46*, 3686–8.

- [54] A. Ghosh, P. Das, M. R. Gill, P. Kar, M. G. Walker, J. A. Thomas, A. Das, *Chem. - A Eur. J.* **2011**, *17*, 2089–2098.
- [55] H. K. Saeed, I. Q. Saeed, N. J. Buurma, J. A. Thomas, *Chem. - A Eur. J.* **2017**, *23*, 5467–5477.
- [56] N. Shan, S. J. Vickers, H. Adams, M. D. Ward, J. A. Thomas, *Angew. Chemie Int. Ed.* **2004**, *43*, 3938–3941.
- [57] N. Shan, J. D. Ingram, T. L. Easun, S. J. Vickers, H. Adams, M. D. Ward, J. a Thomas, *Dalton Trans.* **2006**, 2900–6.
- [58] A. Zubi, A. Wragg, S. Turega, H. Adams, P. J. Costa, V. Félix, J. A. Thomas, *Chem. Sci.* **2015**, *6*, 1334–1340.
- [59] A. Kaifer, L. Echegoyen, D. A. Gustowski, D. M. Goli, G. W. Gokel, *J. Am. Chem. Soc.* **1983**, *105*, 7168–7169.
- [60] A. Kaifer, D. A. Gustowski, L. Echegoyen, V. J. Gatto, R. A. Schultz, T. P. Cleary, C. R. Morgan, D. M. GOLI, A. M. Rios, G. W. Gokel, *J. Am. Chem. Soc.* **1985**, *107*, 1958–1965.
- [61] C. D. Hall, N. W. Sharpe, I. P. Danks, Y. P. Sang, *J. Chem. Soc. Chem. Commun.* **1989**, 419–421.
- [62] J. C. Medina, T. T. Goodnow, S. Bott, J. L. Atwood, A. E. Kaifer, G. W. Gokel, *J. Chem. Soc. Chem. Commun.* **1991**, 290–292.
- [63] J. C. Medina, T. T. Goodnow, M. T. Rojas, J. L. Atwood, B. C. Lynn, A. E. Kaifer, G. W. Gokel, *J. Am. Chem. Soc.* **1992**, *114*, 10583–10595.
- [64] Y. Haketa, H. Maeda, *Chem. - A Eur. J.* **2010**, *17*, 1485–1492.
- [65] Y. Hua, Y. Liu, C.-H. Chen, A. H. Flood, *J. Am. Chem. Soc.* **2013**, *135*, 14401–14412.
- [66] J. Cai, J. L. Sessler, *Chem. Soc. Rev.* **2014**, *43*, 6198–6213.
- [67] B. L. Schottel, H. T. Chifotides, K. R. Dunbar, *Chem. Soc. Rev.* **2008**, *37*, 68–83.
- [68] R. E. Dawson, A. Hennig, D. P. Weimann, D. Emery, V. Ravikumar, J. Montenegro, T. Takeuchi, S. Gabutti, M. Mayor, J. Mareda, C. A. Schalley, S. Matile, *Nat. Chem.* **2010**, *2*, 533–538.
- [69] H. T. Chifotides, K. R. Dunbar, *Acc. Chem. Res.* **2012**, *46*, 894–906.
- [70] D.-X. Wang, M.-X. Wang, *J. Am. Chem. Soc.* **2013**, *135*, 892–897.
- [71] M. Giese, M. Albrecht, K. Rissanen, *Chem. Rev.* **2015**, *115*, 8867–8895.
- [72] M. J. Frisch, G. W. Trucks, H. B. Schlegel, G. E. Scuseria, M. A. Robb, J. R. Cheeseman, G. Scalmani, V. Barone, B. Mennucci, G. A. Petersson, H. Nakatsuji, M. Caricato, X. Li, H. P. Hratchian, A. F. Izmaylov, J. Bloino, G. Zheng, J. L. Sonnenberg, M. Hada, M. Ehara, K. Toyota, R. Fukuda, J. Hasegawa, M. Ishida, T. Nakajima, Y. Honda, O. Kitao, H. Nakai, T. Vreven, J. A. Montgomery Jr, J. E. Peralta, F. Ogliaro, M. J. Bearpark, J. Heyd, E. N. Brothers, K. N. Kudin, V. N. Staroverov, R. Kobayashi, J. Normand, K. Raghavachari, A. P. Rendell, J. C. Burant, S. S. Iyengar, J. Tomasi, M. Cossi, N. Rega, N. J. Millam, M. Klene, J. E. Knox, J. B. Cross, V. Bakken, C. Adamo, J. Jaramillo, R. Gomperts, R. E. Stratmann, O. Yazyev, A. J. Austin, R. Cammi, C. Pomelli, J. W. Ochterski, R. L. Martin, K. Morokuma, V. G. Zakrzewski, G. A. Voth, P. Salvador, J. J. Dannenberg, S. Dapprich, A. D. Daniels, Ö. Farkas, J. B. Foresman, J. V. Ortiz, J. Cioslowski, D. J. Fox, *Gaussian, Revis. D.* **2009**.
- [73] B. Mennucci, J. Tomasi, R. Cammi, J. R. Cheeseman, M. J. Frisch, F. J. Devlin, S. Gabriel, P. J. Stephens, *J. Phys. Chem. A* **2002**, *106*, 6102–6113.
- [74] S. Grimme, S. Ehrlich, L. Goerigk, *J. Comput. Chem.* **2011**, *32*, 1456–1465.
- [75] L. E. Roy, P. J. Hay, R. L. Martin, *J. Chem. Theory Comput.* **2008**, *4*, 1029–1031.
- [76] T. Lu, F. Chen, *J. Comput. Chem.* **2011**, *33*, 580–592.
- [77] T. Lu, F. Chen, *J. Mol. Graph. Model.* **2012**, *38*, 314–323.
- [78] R. F. W. Bader, *Acc. Chem. Res.* **1985**, *18*, 9–15.
- [79] R. F. W. Bader, *Chem. Rev.* **1991**, *91*, 893–928.
- [80] F. Weinhold, C. R. Landis, *Chem. Educ. Res. Pr.* **2001**, *2*, 91–104.
- [81] E. D. Glendening, C. R. Landis, F. Weinhold, *J. Comput. Chem.* **2013**, *34*, 1429–1437.
- [82] E. Espinosa, E. Molins, C. Lecomte, *Chem. Phys. Lett.* **1998**, *285*, 170–173.
- [83] V. K. Davis, C. M. Bates, K. Omichi, B. M. Savoie, N. Momčilović, Q. Xu, W. J. Wolf, M. A. Webb, K. J. Billings, N. H. Chou, S. Alayoglu, R. K. McKenney, I. M. Darolles, N. G. Nair, A. Hightower, D. Rosenberg, M. Ahmed, C. J. Brooks, T. F. Miller, R. H. Grubbs, S. C. Jones, *Room-Temperature Cycling of Metal Fluoride Electrodes: Liquid Electrolytes for High-Energy Fluoride Ion Cells*, **2018**.
- [84] E. S. Böes, P. R. Livotto, H. Stassen, *Chem. Phys.* **2006**, *331*, 142–158.
- [85] C. G. Zhan, D. A. Dixon, *J. Phys. Chem. A* **2004**, *108*, 2020–2029.
- [86] C. L. D. Gibb, B. C. Gibb, *J. Am. Chem. Soc.* **2011**, *133*, 7344–7347.
- [87] P. S. Cremer, A. H. Flood, B. C. Gibb, D. L. Mobley, *Nat. Chem.* **2018**, *10*, 8–16.
- [88] T. Koopmans, *Physica* **1934**, *1*, 104–113.
- [89] I. K. Petrushenko, *Adv. Mater. Sci. Eng.* **2015**, *2015*, 1–7.
- [90] W. Kunz, J. Henle, B. W. Ninham, *Curr. Opin. Colloid Interface Sci.* **2004**, *9*, 19–37.
- [91] Y. Liu, A. Sengupta, K. Raghavachari, A. H. Flood, *Chem.* **2017**, *3*, 411–427.
- [92] L. M. Eytel, H. A. Fargher, M. M. Haley, D. W. Johnson, *Chem. Commun.* **2019**, *55*, 5195–5206.
- [93] R. H. Fish, G. Jaouen, *Organometallics* **2003**, *22*, 2166–2177.
- [94] N. Christinat, R. Scopelliti, K. Severin, *Angew. Chemie Int. Ed.* **2008**, *120*, 1874–1878.
- [95] A. Granzhan, C. Schouwey, T. Riis-Johannessen, R. Scopelliti, K. Severin, *J. Am. Chem. Soc.* **2011**, *133*, 7106–7115.

WILEY-VCH